Soil & Tillage Research 175 (2018) 267–275

Contents lists available at ScienceDirect

Soil & Tillage Research

journal homepage: www.elsevier.com/locate/still

Evaluating calibration methods for predicting soil available nutrients using hyperspectral VNIR data

Haijun Qi[a,c], Tarin Paz-Kagan[b], Arnon Karnieli[c], Xiu Jin[a], Shaowen Li[a,*]

[a] School of Information and Computer Science, Anhui Agricultural University, Hefei 230036, China
[b] Department of Sensing, Information and Mechanization Engineering, Institute of Agricultural Engineering, Agricultural Research Organization (ARO), Volcani Center, Israel
[c] The Remote Sensing Laboratory, Jacob Blaustein Institutes for Desert Research, Ben-Gurion University of the Negev, Sede Boqer Campus 84990, Israel

ARTICLE INFO

Keywords:
Spectral analysis
Soil measurements
Prediction methods
Calibration
Regression algorithms

ABSTRACT

Soil nutrients, including available nitrogen (N), phosphorous (P), and potassium (K), are critical properties for monitoring soil fertility and function. Spectroscopy analysis has proven to be a rapid and effective means for predicting soil properties, in general, and NPK, in particular. However, different calibration methods, including preprocessing transformations (PPTs) and regression algorithms (RAs), considerably affect the performance of prediction models. In this study, raw spectrum and 21 PPTs, combined with three RAs, for a total of 66 calibration methods, were investigated for modeling and predicting soil NPK using hyperspectral VNIR data (400–1000 nm). The ratio of performance to deviation (RPD) of validation set was selected to evaluate the prediction accuracy and the ratio between the interpretable sum squared deviation and the real sum squared deviation (SSR/SST) of the validation set was also used to evaluate the explanatory power of the models. It was found that there is a tradeoff between RPD and SSR/SST values; under this tradeoff, the multiplicative scatter correction, combined with the back-propagation neural network, was preferred for predicting P (RPD = 2.23, SSR/SST = 0.81). The Savitzky-Golay filtering + logarithmic transformation, combined with the partial least squares – regression, was preferred for predicting K (RPD = 1.47, SSR/SST = 0.95). However, with extremely low RPD and SSR/SST values, the prediction of N was unreliable in this study. The evaluation approach presented in this paper suggests a framework for choosing a calibration method for spectroscopy analysis for predicting soil NPK and perhaps some other properties.

1. Introduction

Soil available nutrients, including available nitrogen, phosphorus, and potassium (NPK), playing an important role in enhancing soil fertility and plant productivity for the growth and development of agricultural systems. Wheat and corn are important grain crops in Anhui Province, China, and in many other regions across the globe with high NPK demand. However, excessive fertilization not only affects soil fertility and increases the economic investment, but it also leads to environmental pollution (e.g., Chen et al., 2009; Sadowski et al., 1987; Savci, 2012). It is essential to improve the efficiency and accuracy of soil available nutrient detection for the reasonable fertilization and the sustainable development of agricultural systems. Traditional laboratory methods for quantifying NPK are expensive and time-consuming, and thus cannot meet the requirements of modern soil quality assessment and management, particularly with respect to precision agriculture. Alternatively, previous studies have suggested the reflectance spectroscopy analysis approach as a rapid, non-destructive, reproducible, and cost-effective analytical method for assessing soil properties (Ben-Dor and Banin, 1995).

Reflectance spectroscopy is used in chemometrics to construct soil spectral classification and regression models to predict many soil attributes. Several soil properties with high concentration have a specific spectral absorption signal that can be well predicted with the reflectance spectroscopy analysis approach. For example, soil water content has significant absorption bands around 1400 and 1900 nm (Stoner and Baumgardner, 1980). Organic matter has broad sensitive bands from the visible to the shortwave infrared range (350–2500 nm) due to the overtones and combination absorptions of O−H, C−H, and N−H bonds (Clark et al., 1990). The most common sensitive bands associated with clay minerals are the 1400–1410 and 2160–2200 nm due to the metal−OH band plus the O−H stretch combination and C−O (Galvão et al., 1997; Hunt and Salisbury, 1970). Unfortunately, soil NPK do not have any obvious spectral feature and usually exist in low

* Corresponding author.
E-mail addresses: shwli@ahau.edu.cn, shwli2017@163.com (S. Li).

http://dx.doi.org/10.1016/j.still.2017.09.006
Received 7 August 2017; Received in revised form 10 September 2017; Accepted 14 September 2017
0167-1987/ © 2017 Elsevier B.V. All rights reserved.

Table 1
Summary of previous research results for predicting NPK by various calibration methods.

Literature	Spectral range	Calibration method		Nutrient	Results
		PPT	RA		
Confalonieri et al. (2001)	1100–2498 nm	LG	Modified PLS-R	P	R^2 = 0.23–0.57
				K	R^2 = 0.48–0.82
Viscarra Rossel et al. (2006)	400–14286 nm	LG	PLS-R	NO_3^--N	R^2_{adj} = −0.02–0.00
				P	R^2_{adj} = 0.01–0.20
				K	R^2_{adj} = 0.29–0.47
Mouazen et al. (2010)	350–2500 nm	5 points averaged + normalization + SG + FD	BPNN-LVs	P/K	R^2 = 0.68–0.74, RPD = 1.77–1.94
Shao and He (2011)	800–2500 nm	SG + MSC	LS-SVM	N	r = 0.90
				P	r = 0.83
				K	r = 0.83
	4000–400 cm^{-1}	SG + MSC	LS-SVM	N	r = 0.87
				P	r = 0.88
				K	r = 0.89
Gholizade et al. (2013)	700–2500 nm	SG + SD	SMLR	P	R^2 = 0.52
				K	R^2 = 0.48
Wu et al. (2014)	350–2500 nm	MSC + FD	Global BPNN	N	r = 0.78
				P	r = 0.65
				K	r = 0.86
			Local BPNN	N	r = 0.90
				P	r = 0.82
				K	r = 0.94
Ji et al. (2014)	350–2500 nm	LG + SG	PLS-R	N	R^2 = 0.86, RPD = 2.49
				P	R^2 = 0.29, RPD = 1.17
				K	R^2 = 0.07, RPD = 0.77
			LS-SVM (in situ spectrum)	N	R^2 = 0.76, RPD = 1.91
				P	R^2 = 0.36, RPD = 1.27
				K	R^2 = 0.14, RPD = 0.91
Paz-Kagan et al. (2014), Paz-Kagan et al. (2015)	350–2500 nm	SG + auto scale + generalized least squares weighting	PLS-R	NH_4^+-N	R^2 = 0.27–0.83, RPD = 1.69–2.43
				NO_3^--N	R^2 = 0.74–0.82, RPD = 1.76–2.68
				P	R^2 = 0.21–0.74, RPD = 0.53–1.98
				K	R^2 = 0.61–0.76, RPD = 2.00–2.25
Hu et al. (2016)	350–2500 nm	LG + normalization + 5 points averaged	PLS-R	P	R^2 = 0.35, RPD = 1.20
				K	R^2 = 0.42, RPD = 1.24
		LG + normalization + 5 points averaged + DOSC	PLS-R	P	R^2 = 0.63, RPD = 1.64
				K	R^2 = 0.66, RPD = 1.72
Sarathjith et al. (2016)	350–2500 nm	FD + WT	SVM	P	R^2 = 0.80, RPD = 2.27
				K	R^2 = 0.71, RPD = 1.89
Yu et al. (2016)	350–2500 nm	SG + LG + FD	SMLR + spectral index	NH_4^+-N	R^2 = 0.74–0.92, RPD = 1.89–3.49
				NO_3^--N	R^2 = 0.33–0.53, RPD = 1.02–1.37
				P	R^2 = 0.44–0.51, RPD = 1.29–1.37
				K	R^2 = 0.51–0.95, RPD = 1.32–4.26
			PLS-R + spectral index	NH_4^+-N	R^2 = 0.78–0.92, RPD = 2.06-3.40
				NO_3^--N	R^2 = 0.30–0.73, RPD = 0.95–1.89
				P	R^2 = 0.39–0.51, RPD = 1.17–1.38
				K	R^2 = 0.37–0.71, RPD = 1.15–1.59
Shaddad et al. (2016)	350–2500 nm	3 points averaged + normalization + SG + FD	PLS-R	P	R^2 = 0.77, RPD = 2.08
				K	R^2 = 0.55, RPD = 1.48

Abbreviations used: preprocessing transformation (PPT); regression algorithm (RA); logarithmic transformation (LG); first derivative (FD); Savitzky-Golay filtering (SG); multiplicative scatter correction (MSC); wavelet transformation (WT); direct orthogonal signal correction (DOSC); partial least squares − regression (PLS-R); back-propagation neural network (BPNN); least squares − support vector machine (LS-SVM); stepwise multiple linear regression (SMLR); support vector machine (SVM); available nitrogen (N); available phosphorous (P); available potassium (K); ammonium nitrogen (NH_4^+-N); nitrate nitrogen (NO_3^-N); coefficient of determination (R^2); correlation coefficient (r); the ratio of performance to deviation (RPD).

concentrations in the soil (Ji et al., 2014). Consequently, their identification using spectral approach (calibration and prediction) is difficult to achieve. In addition, the existence of unexpected irrelevant information in spectra also greatly affects the performance of calibration models for quantifying soil NPK.

Calibration methods, including different combinations of preprocessing transformations (PPTs) and regression algorithms (RAs) have been widely applied to improve the prediction accuracy of soil NPK. PPTs, based on various mathematical functions, can be used to correct for non-linearity, measurement and sample variations, and

noisy spectra (Stenberg et al., 2010). RAs also play an important role in calibration to model the complex relationship between spectra and NPK (Soriano-Disla et al., 2014). Table 1 summarizes the results of past studies for predicting NPK by various calibration methods with the spectroscopy analysis approach. The prediction results show high variations that are greatly affected by the selected calibration methods and the spectral range. Many of these methods are useful, but still some are ineffective. Therefore, it is essential to compare the performances of different calibration methods and to optimize the best ones for predicting NPK, individually. Table 1 shows that the prediction of soil NPK using spectroscopy in the region of visible near infrared to shortwave infrared (VNIR-SWIR, 400–2500 nm) is feasible. Compared to the VNIR-SWIR sensors, the hyperspectral sensors within the VNIR (400–1000 nm) region are more economical and accessible with higher signal to noise ratio (SNR). However, to the best of our knowledge, the application of hyperspectral VNIR data, especially with imaging spectrometer, to predict soil NPK has been relatively scarce, although it has been successfully used for predicting other soil properties such as soil organic matter and carbon fractions (e.g., Adar et al., 2014; Jung et al., 2015; O'Rourke and Holden, 2012), soil biochar (e.g., Tong et al., 2013), total nitrogen (e.g., Buddenbaum and Steffens, 2012; Li et al., 2015), and more. Furthermore, the application of hyperspectral imaging VNIR data would make this technology accessible for the large scale mapping and monitoring of soil NPK using airborne and spaceborne platforms (Adar et al., 2014).

Several researchers (e.g., Mouazen et al., 2010; Sarathjith et al., 2016; Shao and He, 2011; Yu et al., 2016) focused on comparing the prediction accuracy of different calibration methods by coefficient of determination (R^2), the ratio of performance to deviation (RPD), root mean square error (RMSE), correlation coefficient (r), etc. However, high prediction accuracy may only indicate a good agreement between the predicted and measured values in the special validation set. The extremely high prediction accuracy probably results from overfitting of the calibration model (Peng, 2010). In the multivariate calibration of a soil spectroscopy analysis, the emphasis on causal explanation versus empirical prediction is more mixed. Thus, the performance of explanatory power should also be considered (Shmueli, 2010). The spectral features of soil NPK are indirectly associated with the vibration modes of functional groups, such as OH^-, SO_4^{2-}, CO_3^{2-} and their combinations (Ben-Dor and Banin, 1995). The calibration models should carry more relationships or underlying constructs between multi-spectral features to shed light on the concentrations of predicted soil available nutrients (Osborne, 2000). The primary goal of a good calibration model is to achieve a high RPD to confirm the prediction accuracy (in general, RPD > 2). In addition, the model should also receive more statistical information from testing samples to ensure high explanatory power (e.g., Peng, 2010; Wen et al., 2008).

The current study's aims are the following: (1) to investigate the predictive ability of hyperspectral visible-near infrared data (400–1000 nm) for predicting soil available nitrogen, phosphorus, and potassium (NPK) in lime concretion black soil; and (2) to evaluate the performance of different calibration methods, including 21 preprocessing transformations (PPTs) and 3 regression algorithms (RAs), with respect to both prediction accuracy and explanatory power.

2. Materials and methods

2.1. Study area and soil sampling

The sampling was conducted in three sites in the plain of northern Anhui Province, China. The plain lies in the warm-temperate semi-humid monsoon climate zone, which was produced by the sediments and alluvial deposits of the Huaihe River and its tributaries (Ma et al., 2014). The main soil type in this area is lime concretion black soil, and a wheat-maize rotation is the main cropping system. Due to the poor soil quality, fertilization is extremely important in these soils (Chen et al., 2014). Thus, research sites have been established to amend the soil with optimized fertilization. Although the study areas have the same terrain and the same soil type, historically different land-use types (wheat cultivation, vegetable cultivation, grass, and wasteland) and different treatments (variable fertilization, variable straw returning and variable planting density) have resulted in significant data variation of the available nutrient contents. Soil samples were collected at a depth of 0–20 cm from May to June 2016 after the wheat harvest and before the planting and fertilization for maize, with a mean daily temperature ranging from 27 to 30 °C. For each sample, there were three sampling points in a diagonal across each sampling field; about 1.5 kg of pure soil remained after removing stones, straws, and roots. In total, 153 samples were collected for analysis.

2.2. Physicochemical lab analysis

Each sample was labeled and taken to the laboratory for air drying in a natural, windless 24 °C indoor environment for one month. After air-drying, impurities-removing (e.g. residual dry vegetation, rock particles), grinding and sieving (< 2 mm), each sample was divided into two parts. One part was designated for standard chemical laboratory analysis and the other for hyperspectral VNIR acquisition. The chemical analysis for N was performed with the alkali-hydrolyzed diffusing absorption method, P was measured with the sodium hydrogen carbonate solution–Mo–Sb anti-spectrophotometric method, and K was measured with the ammonium acetate extraction-flame photometric detection method (Lu, 2000). The outliers were determined by boxplot (McGill et al., 1978), and eight samples with extremely large N concentrations beyond the upper whisker were removed. Boxplots of the measured NPK concentrations of 145 samples used in calibration and validation are presented in Fig. 1. The results showed high variation in the soil NPK with a significant range of change in all three components, indicating that this data could be used for the regression analysis.

2.3. Laboratory spectral measurements

The laboratory soil spectral data were acquired with an indoor hyperspectral VNIR system. The system consisted of the following parts: a pushbroom-type hyperspectral imager (OKSI, Torrance, CA, USA), a rotation stage with a pan/tilt head for scanning, an illumination source including two halogen lamps (50 W), a Dell Precision Workstation with the data collection software HyperVision, and a set of height-adjustable mounting brackets.

The measurements were conducted in a darkroom to avoid interference of stray light. The soil sample was contained in a Petri dish (diameter of 90 mm and thickness of 15 mm) and placed in a fixed location, and a piece of black light-absorbing cloth was placed under the targeted object as background. The bidirectional and stable

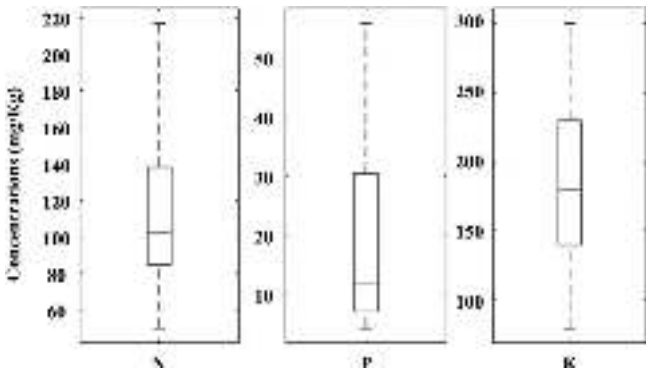

Fig. 1. Boxplots of measured NPK concentrations. The box boundaries represent the 25th and 75th percentiles, the solid lines within boxes represent the median value, and the whiskers represent minimum and maximum values.

illumination reduced the effect of shadowing. In addition, each sample was rotated 90 ° four times for measurements in four directions to reduce the effect of micro-topography shadowing. Thus, the averaged data of four directions were the final outputs for each soil sample (Paz-Kagan et al., 2015). The outputs of this system created "image cubes" of soil samples that consisted of a two-dimensional spatial image (1620 × 841 pixels) with spectral data (400–1000 nm and 1.79 nm resolution, 339 wavebands) at each pixel. Before each soil sample measurement, the hyperspectral imager was calibrated to the spectral reflectance with a standard white reference panel made of pressed and sintered polytetrafluorethylene (Labsphere, North Sutton, NH, USA).

A region of interest (ROI) was selected from the hyperspectral image of the soil sample in a Petri dish. The soil sample was segmented artificially from the one hyperspectral image using the ENVI software (Exelis Visual Information Solutions, Boulder, CO, USA). The spectrum of the ROI was averaged as the research basis (e.g., Cen et al., 2016; Rourke and Holden, 2012) for predicting soil available nutrient content. Considering that all samples had the same fixed position and illumination for collection, the remaining image cubes, including the image cubes of the white reference panel, were also segmented with the same ROI using a self-compiled IDL code (Dong et al., 2015).

2.4. Preprocessing transformations (PPTs)

The reflectance in each pixel of the ROI was averaged as the analytical basis. The wavelengths at both ends that had a significant low SNR were removed to reduce the effect of prediction accuracy. The resultant reflectance spectrum of 303 wavebands (420–960 nm) was used henceforth. In order to eliminate or minimize the additive and multiplicative effects caused, for example, by the heterogeneity of sample texture and physical properties (Osborne et al., 1993), a series of frequently used preprocessing transformations and their integrated methods were applied to the spectral reflectance as follows.

Several commonly used PPTs were tested in this study, including the Savitzky-Golay filtering algorithm (SG) (Savitzky and Golay, 1964) with a second-order polynomial that was selected to smooth the spectral reflectance. A first derivative (FD) and a second derivative (SD) were conducted to remove the baseline and improve the linear trend (e.g., Rinnan et al., 2009; Roberts et al., 2004). A multiplicative scatter correction (MSC) and a standard normal variate (SNV) (e.g., Gholizadeh et al., 2015; Helland et al., 1995) were performed to correct additive and multiplicative effects. A continuous wavelet transformation (WT) (e.g., Ma and Shao, 2004; Peng et al., 2013) was performed to enhance the features in the spectrum. A logarithmic transformation (LG, based on 10) was used to transform reflectance to absorbance and to improve the correlation to sample concentrations (e.g., He et al., 2009; Viscarra Rossel et al., 2006). In addition, the SG was used in conjunction with other methods to obtain an optimal preprocessing method that also has shown to produce good results (e.g., Gholizade et al., 2013; Paz-Kagan et al., 2014; Tian et al., 2013). A total of 21 PPTs, in addition to the raw spectral reflectance (RS), were individually used as input variables for modeling and predicting soil NPK.

2.5. Regression algorithms

As soil NPK may have linear and non-linear relationships with the reflectance or transformed spectrum, commonly used RAs, including the linear algorithm partial least squares − regression (PLS-R), the non-linear intelligent algorithm least squares − support vector machine (LS-SVM), and the back propagation neural network (BPNN), were investigated to develop soil NPK prediction models.

PLS-R is particularly useful for predicting a set of dependent variables from a large set of independent variables (Wold et al., 1983); it has proven to be the most commonly used linear regression technique for predicting soil properties with spectral reflectance (e.g., Paz-Kagan et al., 2015; Shao and He, 2011; Tian et al., 2013; Yu et al., 2016). In the current study, the training X was a matrix of spectral features for the independent variables (size 108 × 303), and the training y was a vector representing one of the soil NPK content for the dependent variables (size 108 × 1). To overcome the collinearity problems between predictors, PLS-R decomposed X and y by linear combinations to extract latent variables (LVs, or components) and built the regression model based on LVs instead of the original training variables (Wold et al., 1984). To avoid over-fitting or under-fitting, a leave-one-out cross-validation was used to determine the number of LVs with the smallest mean squared error and Akaike information criterion (AIC) in calibration (Ji et al., 2014).

LS-SVM regression replaces the convex quadratic programming problem with a convex linear system, solving the problem by replacing the inequality constraints with equality ones, thus largely speeding up the training rate in non-linear regression modeling, especially applicable in high dimensional input spaces (Suykens et al., 2002). In this study, the radial basis function (RBF) kernel was applied. The tuning of the two parameters, the regularization parameter γ and the squared bandwidth σ^2 of the kernel, was conducted in three steps: (1) determining the suitable initial parameters with coupled simulated annealing (CSA) (Xavier-De-Souza et al., 2010); (2) constructing a grid based on CSA starting values; and (3) selecting the best parameters according to the minimum mean squared error in the grid based on a leave-one-out cross-validation (Brabanter et al., 2011).

BPNN is a one-way multi-perceptron feed-forward network (Widyanto et al., 2005) that can be used to calibrate regression models due to its powerful supervised learning ability (Mouazen et al., 2010; Pang et al., 2014). A commonly used three-layer feed-forward network, composed of one input layer (spectral features), one hidden layer (with 10 nodes) and one output layer (one of the soil NPK), was built. The tan-sigmoid and the pure-linear were adopted as the transfer functions in the hidden layer and the output layer. The Bayesian regularization backpropagation (trainbr) was used as the training function, and the maximum value for the Marquardt adjustment parameter was set to 1e-7. The learning rate was set as 0.2, the performance (mse) goal as 0.01 and the maximum number of training epochs as 1000 (Basheer and Hajmeer, 2000).

Hyperspectral VNIR with 303 wavebands as the input spectral features could increase the learning ability of the non-linear intelligent algorithm, but the existence of collinearity and redundancy (Westad et al., 2000) also leads to two overall problems: an extremely long training time and over-fitting. To avoid this, LVs obtained from the PLS-R were adopted as the input spectral features for LS-SVM and BPNN; this proved to be an effective way of reducing computational resources and improving the generalization (e.g., Janik et al., 2007; Morellos et al., 2016; Mouazen et al., 2010).

For the calibration and validation of the regression models, 145 soil samples were divided into two parts with a split ratio of 0.7 to 0.3, respectively, based on the Kennard-Stone algorithm (Kennard and Stone, 1969), conducted on the original spectral matrix. Thus, 102 samples were selected as the calibration set (also used for cross-validation during training) and the remaining 43 as the validation set (independent testing for the established model). To avoid attributes in the higher numerical ranges dominating those in the lower numerical ranges, both the calibration and validation sets were standardized by mapping their mean and standard deviations to 0 and 1, respectively, before calibration and validation (Hsu et al., 2008).

2.6. Accuracy comparison

In order to evaluate the performance of the calibration models, the evaluation criteria were specified as follows. Assuming m is the number of testing samples in the validation set, y_i is the real value of sample i, $f(x_i)$ is the predicted value of sample i, $\bar{y}$ is the average value of y.

The coefficient of determination was used to evaluate the prediction accuracy in the reflectance spectroscopy analysis for a long period (Shmueli, 2010), generally defined as (e.g., Kvalseth, 1985; Weisberg, 2005):

$$R^2 = 1 - \sum_{i=1}^{m} (f(x_i) - y_i)^2 / \sum_{i=1}^{m} (y_i - \bar{y})^2 \quad (1)$$

which was proved to be an inadequate measure for linear no-intercept models and non-linear models (Spiess and Neumeyer, 2010). In this study, the predictive capacities of the calibration models were validated and compared with the ratio of performance to deviation (RPD) of the validation set:

$$RPD = SD/RMSE = \sqrt{m \sum_{i=1}^{m} (y_i - \bar{y})^2 / \sum_{i=1}^{m} (f(x_i) - y_i)^2} / (m - 1) \quad (2)$$

The ratio between the interpretable sum squared deviation and the real sum squared deviation (SSR/SST), which is calculated as:

$$SSR/SST = \sum_{i=1}^{m} (f(x_i) - \bar{y})^2 / \sum_{i=1}^{m} (y_i - \bar{y})^2 \quad (3)$$

was recognized as the proportion of the variability of the response explained by the regression model (e.g., Cope et al., 1991; Peng, 2010; Shmueli, 2010; Weisberg, 2005; Wen et al., 2008).

In most cases, a high RPD value indicates good agreement between estimations and real values; high RPD usually accompanies an increase in the SSR/SST. As mentioned above, an extremely high RPD value may not represent a good model performance, for it probably corresponds to over-fitting. In addition, the RPD value is less sensitive to the presence of compositional outliers (Saeys et al., 2004), especially for very heterogeneous materials, such as soil. Thus, a good calibration model should achieve a higher SSR/SST value under the premise of a high RPD value; in some cases, it is essential to strike a balance between RPD and SSR/SST. In our study, according to (Chang et al., 2001), three categories of predictability were adopted, which are: category A (RPD > 2.0) with good accuracy; category B (1.4 < RPD < 2.0) with moderate accuracy; and category C (RPD < 1.4) with poor accuracy. Usually the SSR/SST should be greater than 0.5 to ensure the stability of the calibration model. All PPTs, RAs and evaluations mentioned above were conducted in MATLAB (MathWorks, Natick, Massachusetts, USA). The LS-SVM regression process was carried out with the LS-SVM toolbox (LS-SVMlab1.8, Suykens, Leuven, Belgium).

3. Results and discussion

3.1. Model performances of different calibration methods

3.1.1. RPD performance

The PPTs provided different prediction accuracies of soil NPK with regard to the RPD values. Fig. 2(a–c) shows the RPD performance with different calibration methods for the prediction of NPK. The prediction accuracy for N was low with an RPD value of less than 1.4 for all the calibration methods (Fig. 2a). The highest value, RPD = 1.05, was obtained with the calibration method of SG + SNV/LS-SVM and SG + MSC/LS-SVM, and all calibration methods were categorized as C (RPD < 1.4). Among the three investigated available nutrients, P (Fig. 2b) was most accurately predicted with a best RPD = 2.29 (SNV/BPNN), categorized as A (RPD > 2). Furthermore, two additional calibration methods fell under category A for predicting P: MSC/BPNN and MSC/LS-SVM. The most suitable calibration method for predicting K, with regard to RPD, was SG + SNV/PLS-R with the best value of RPD = 1.49 (Fig. 2c); this prediction accuracy is categorized as B (1.4 < RPD < 2). Additionally, the accuracies of SG + LG/PLS-R, SG + SNV + FD/LS-SVM and SG + SNV + FD/LS-SVM for predicting K were also categorized as B.

3.1.2. SSR/SST performance

The SSR/SST values of the different calibration methods, which are used to describe the explanatory power of these models, are presented in Table 2. The SSR/SST values of the same available nutrient with different calibration methods tend to, but not always, increase with increasing RPD values. No calibration method achieved a SSR/SST value of more than 0.5 for predicting N. Fig. 2a also shows that all calibration methods fell in category C, proving poor ability to predict N using hyperspectral VNIR data. For the prediction of P, the SSR/SST values varied from 0.06 to 0.57 for the calibration methods in category C, from 0.58 to 1.15 for category B, and from 0.64 to 0.81 for category A. Every calibration method with RPD > 1.4 had an SSR/SST value of more than 0.5; all of these methods are reliable for predicting P by hyperspectral VNIR data, especially those calibration methods in category A, representing good prediction ability. For predicting K, the SSR/SST values varied from 0.00 to 1.06 for the calibration methods in category C, and from 0.58 to 0.95 for category B, confirming the moderate ability to predict K using hyperspectral VNIR data.

3.2. Comparison of different calibration methods

According to Fig. 2 and Table 2, both PPTs and RAs influence the model's performance with regard to RPD and SSR/SST. Similar results have been presented by (e.g., Mouazen et al., 2010; Shi et al., 2013). Gras et al. (2014) also showed that the effect of PPTs on prediction accuracy is particularly important with sieved soil samples. Generally, the most used PPTs perform better than raw spectral reflectance, especially for MSC, SNV and some of their integrated methods. This means that various multiplicative transformations of spectral variables can successfully eliminate the effect of physical phenomena such as the light scattering effect of particles of different sizes and shapes (Helland et al., 1995) in predictions with hyperspectral VNIR data. In addition, SG-filtered PPTs can significantly improve prediction accuracy due to noise removal, especially with linear regression (PLS-R). The use of derivative transformed PPTs can effectively remove the baseline and improve the linear trend. SG + LG and SG + WT also can enhance correlations and perform well. However, direct transformations on unfiltered spectral data perform poorly and may even increase the effect of noise signal. Therefore, PPTs, such as SD, WT, SNV + SD and MSC + SD, for predicting P diminish the model's performance.

PLS-R performed better than LS-SVM and BPNN with most SG-filtered PPTs, and the prediction accuracy of LS-SVM and BPNN with MSC and SNV for predicting P even decreased after SG-filtering. The main reason for this is that, with the reduction of the noise signal, a portion of important corresponding non-linear information was also removed by SG. Nevertheless, it can also be seen that LS-SVM and BPNN achieved higher prediction performances than PLS-R with most unfiltered PPTs, perhaps benefitting from stronger model learning ability and unfiltered non-linear input information. In this study, the input of LS-SVM and BPNN was replaced by selected LVs, which can greatly save training time and improve the generalization performance. However, there is still some weak information existing in unused LVs; neglecting unused LVs may limit the prediction performance's improvement.

3.3. Calibration method selection

Many calibration methods can achieve high prediction accuracy or explanatory power; thus, it is necessary to select the best ones for modeling and predicting soil NPK (Fig. 2 and Table 2). Since both the RPD and SSR/SST values were very small for N, it is assumed that hyperspectral VNIR data have low ability to predict N in this study; this may be because the spectral range is not suitable for N prediction and the SWIR region is required.

The best RPD and the best SSR/SST values usually did not coexist

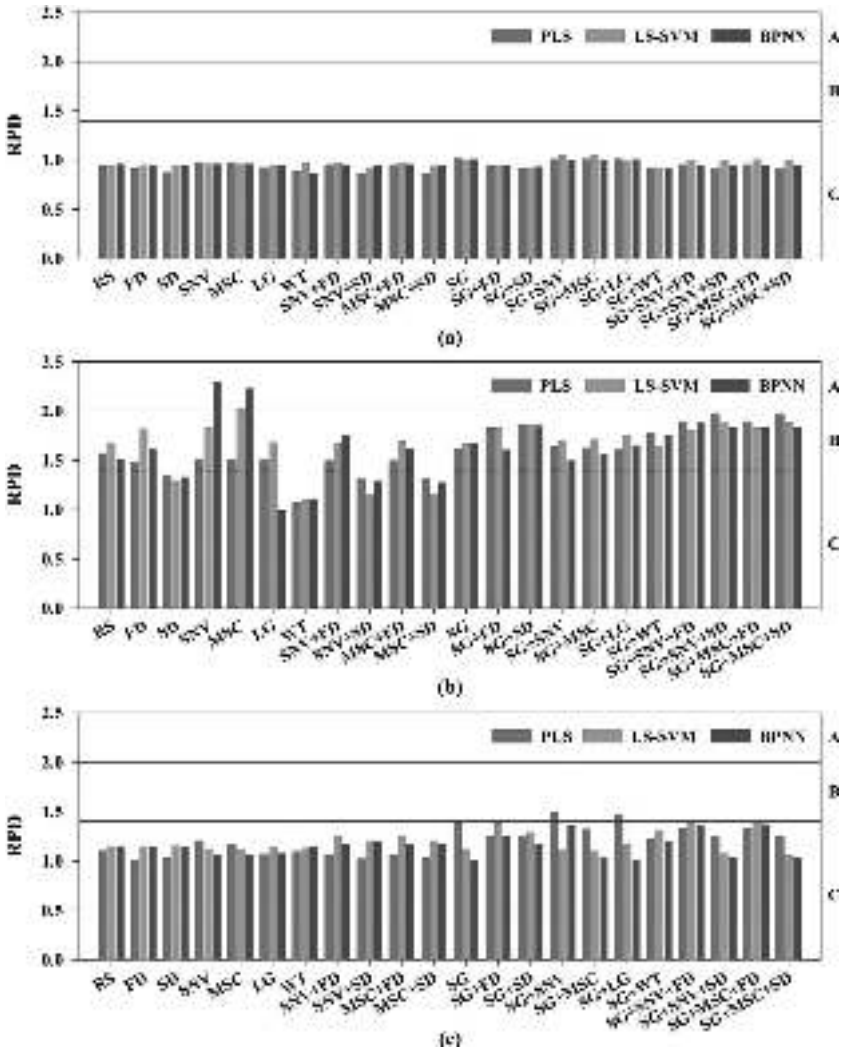

Fig. 2. The ratio of performance to deviation (RPD) values of different calibration methods for the validation set for predicting: (a) available nitrogen (N); (b) available phosphorous (P); and (c) available potassium (K). Category A: RPD > 2.0, category B: 1.4 < RPD < 2.0, category C: RPD < 1.4. Abbreviations used: raw spectral reflectance (RS); Savitzky-Golay filtering (SG); first derivative (FD); second derivative (SD); standard normal variate (SNV); multiplicative scatter correction (MSC); logarithmic transformation (LG, based on 10); wavelet transformation (WT); partial least squares – regression (PLS-R); least squares – support vector machine (LS-SVM); back-propagation neural network (BPNN).

within the same calibration method. For the prediction of P, the best RPD value was obtained by the SNV/BPNN calibration method, while the best SSR/SST value was obtained by RS/BPNN. For the prediction of K, the best RPD value was obtained by SG + SNV/PLS-R, while the best SSR/SST value was obtained by SG + WT/PLS-R. In addition, the next-best RPD with the high SSR/SST value should also be noted. These special calibration methods are recognized as the candidate calibration methods and should be especially considered in hyperspectral VNIR analyses. The candidates and their performances are summarized in Table 3.

To compare the comprehensive performances for predicting P and K using these candidates, Fig. 3a, b presents the scatterplots and univariate linear regression lines of the predicted values versus the measured values of P and K, respectively. As can be seen in Fig. 3, the scatterplot seems more centralized around the univariate linear regression line with a higher RPD value, indicating high prediction accuracy. The slope of the regression line generally increases with the SSR/SST value indicating high explanatory power. If the SSR/SST value is extremely large (even more than 1) and the RPD is very small, the scatterplot would be much more discrete caused by outliers. If the RPD value is extremely large and the SSR/SST is very small, the regression line would be much tilted. For a good calibration method, the regression line of the measured values and the predicted values should approach y = x (1:1), also meaning the slope is closer to 1. In this case, as the number of test samples increase, the new scatterplots would also distribute around y = x, which means this calibration model has a high stability. Of course, the premise is that the scatterplot should be more centralized to ensure prediction accuracy. Hence, both the RPD and SSR/SST values are important in evaluating the performance of different calibration methods.

The RS/BPNN calibration method for predicting P has the highest slope of 0.86 caused by the highest SSR/SST value of 1.15. However, the scatterplot is more discrete due to the lowest RPD value of 1.51. The RPD value of MSC/BPNN is 2.23, very close to the RPD value of SNV/BPNN at 2.29. Therefore, SNV/BPNN is abandoned due to its lowest slope of 0.80. Consequently, MSC/BPNN would be the most suitable calibration method for predicting P benefit from the higher slope of 0.81. For K prediction, the scatterplot of SG + WT/PLS-R is very discrete due to the lowest RPD of 1.21. The SG + LG/PLS-R performed better than SG + SNV/PLS-R, benefitting from the highest slope of 0.74 and the higher SSR/SST value of 0.95; this could be a suitable calibration method for predicting K.

4. Conclusions

The current paper illustrates that prediction performance can be significantly improved by applying proper calibration methods. The SG-filtered PPTs, such as derivative transformations and scatter correction

Table 2
Ratios between the interpretable sum squared deviation and the real sum squared deviation (SSR/SST) of different calibration methods.

Calibration method	N			P			K		
	PLS-R	LS-SVM	BPNN	PLS-R	LS-SVM	BPNN	PLS-R	LS-SVM	BPNN
RS	0.08	0.08	0.04	**0.73**	**0.74**	**1.15**$^{\#}$	0.16	0.20	0.22
FD	0.15	0.04	0.05	**0.85**	**0.58**	**0.67**	0.52	0.42	0.49
SD	0.32	0.08	0.08	0.43	0.26	0.29	0.60	0.37	0.39
SNV	0.08	0.07	0.06	**0.74**	**0.64**	**0.76***	0.22	0.19	0.13
MSC	0.08	0.07	0.06	**0.75**	**0.65**	**0.81**	0.31	0.20	0.12
LG	0.08	0.06	0.05	**0.80**	**0.76**	0.06	0.22	0.22	0.17
WT	0.28	0.10	0.24	0.57	0.51	0.48	0.42	0.28	0.27
SNV + FD	0.24	0.13	0.05	**0.85**	**0.63**	**0.61**	0.43	0.43	0.57
SNV + SD	0.41	0.13	0.05	0.25	0.49	0.20	0.57	0.42	0.49
MSC + FD	0.24	0.16	0.05	**0.85**	**0.61**	**0.58**	0.43	0.42	0.58
MSC + SD	0.42$^{\#}$	0.13	0.07	0.25	0.46	0.26	0.57	0.43	0.48
SG	0.11	0.09	0.00	**0.76**	**0.67**	**0.78**	0.99	0.57	0.00
SG + FD	0.09	0.04	0.04	**0.75**	**0.83**	**0.96**	0.90	0.66	0.96
SG + SD	0.13	0.09	0.06	**0.78**	**0.68**	**0.70**	0.97	0.83	1.04
SG + SNV	0.09	0.15*	0.08	**0.72**	**0.62**	**0.80**	**0.74***	0.48	0.91
SG + MSC	0.09	0.15*	0.08	**0.73**	**0.62**	**0.84**	1.05	0.42	0.02
SG + LG	0.10	0.07	0.00	**0.77**	**0.71**	**0.78**	**0.95**	0.51	0.01
SG + WT	0.26	0.15	0.15	**0.68**	**0.68**	**0.71**	1.06$^{\#}$	0.77	0.93
SG + SNV + FD	0.06	0.04	0.04	**0.71**	**0.72**	**0.70**	0.74	**0.59**	0.65
SG + SNV + SD	0.21	0.14	0.04	**0.74**	**0.67**	**0.67**	0.94	0.80	0.04
SG + MSC + FD	0.06	0.05	0.04	**0.71**	**0.69**	**0.73**	0.74	0.58	0.65
SG + MSC + SD	0.21	0.15	0.04	**0.74**	**0.69**	**0.67**	0.93	0.85	0.03

Bold underlined values indicate the ratio of performance to deviation (RPD) > 2.0 corresponding to category A, bold values indicate 1.4 < RPD < 2.0 corresponding to category B, and the remaining values indicate RPD < 1.4 corresponding to category C; numbers with ($^{\#}$) correspond to the best of the ratio between the interpretable sum squared deviation and the real sum squared deviation (SSR/SST) values; numbers with (*) correspond to the best RPD values. Abbreviations used: available nitrogen (N); available phosphorous (P); available potassium (K); raw spectral reflectance (RS); Savitzky-Golay filtering (SG); first derivative (FD); second derivative (SD); standard normal variate (SNV); multiplicative scatter correction (MSC); logarithmic transformation (LG, based on 10), wavelet transformation (WT), partial least squares − regression (PLS-R); least squares − support vector machine (LS-SVM); back-propagation neural network (BPNN).

Table 3
Candidate calibration methods and their performances.

Property	Calibration method		Performance				Remark
	PPT	RA	Calibration		Validation		
			RPD	SSR/SST	RPD	SSR/SST	
P	RS	BPNN	3.26	0.84	1.51	1.15	Best SSR/SST
	SNV	BPNN	3.10	0.86	2.29	0.76	Best RPD
	MSC	BPNN	2.59	0.82	2.23	0.81	Next-best RPD
K	SG + SNV	PLR-R	1.54	0.58	1.49	0.74	Best RPD
	SG + LG	PLR-R	1.65	0.63	1.47	0.95	Next-best RPD
	SG + WT	PLR-R	1.83	0.70	1.21	1.06	Best SSR/SST

Abbreviations used: available phosphorous (P); available potassium (K); preprocessing transformation (PPT); regression algorithm (RA); raw spectral reflectance (RS); Savitzky-Golay filtering (SG); standard normal variate (SNV); multiplicative scatter correction (MSC); logarithmic transformation (LG, based on 10); wavelet transformation (WT); partial least squares − regression (PLS-R); back-propagation neural network (BPNN); the ratio of performance to deviation (RPD); the ratio between the interpretable sum squared deviation and the real sum squared deviation (SSR/SST).

methods, showed higher performances both in linear and non-linear RAs, especially for PLS-R. But non-linear intelligent RAs work better than PLS-R with some special unfiltered PPTs. As a result, hyperspectral VNIR data (400–1000 nm) showed good ability for predicting P, moderate ability for predicting K, and poor ability for predicting N. The results further show that both RPD and SSR/SST are important in evaluating the performance of calibration models. As the two indices may not achieve their best values simultaneously, this study constructed detailed evaluation criteria for various calibration methods as follows:

1) Classify RPD values into different categories of predictability: category A (RPD > 2.0) with good accuracy; category B (1.4 < RPD < 2.0) with moderate accuracy; and category C (RPD < 1.4) with poor accuracy (Chang et al., 2001).
2) Compare the SSR/SST values between calibration methods using the same categories according to step 1, and select calibration methods with high SSR/SST values or high RPD values as candidate calibration methods. Usually the SSR/SST value should be greater than 0.5.
3) Regress and scatterplot the measured values and the predicted values of each sample in the validation set of the candidate calibration methods from step 2. Conduct a tradeoff by comparing the distribution of the scatterplots and selecting the best fit model with low visual deviation.

According to numerical and visual tradeoffs, MSC/BPNN (RPD = 2.23, SSR/SST = 0.81) and SG + LG/PLS-R (RPD = 1.47, SSR/SST = 0.95) are selected as the most suitable methods for predicting P and K, respectively, in this study.

The current study suggests a framework for using hyperspectral VNIR data to select calibration methods and improve the ability to predict soil NPK. This framework can be applied for predicting various soil properties that meet the requirements of modern soil quality assessment and management. Further works should examine additional calibration methods and pay more attention to optimizing these methods to improve both RPD and SSR/SST values. In addition, the number of soil samples and soil types should also be increased to make the calibration methods more stable and robust; the relationship between soil spectral characteristics and chemical components should also be investigated to understand the prediction mechanism.

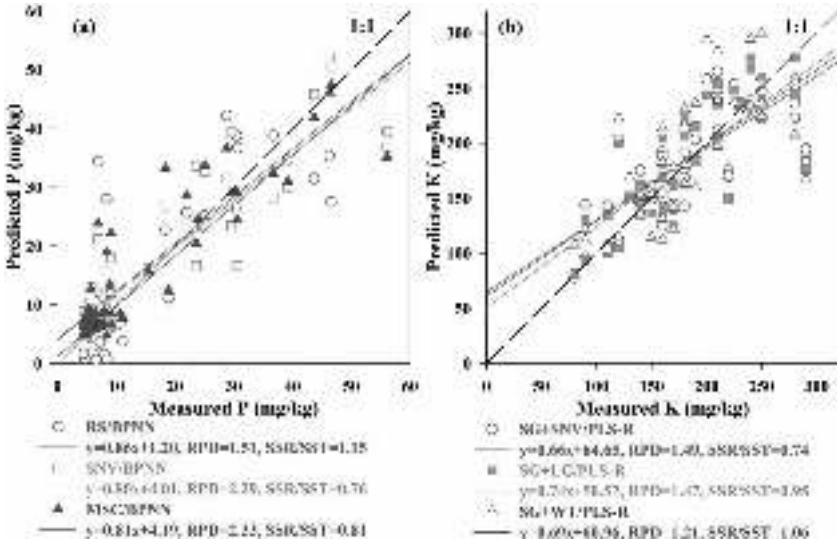

Fig. 3. Predicted versus measured values for (a) available phosphorous (P) and (b) available potassium (K) with several selected calibration methods. Abbreviations used: raw spectral reflectance (RS); Savitzky-Golay filtering (SG); standard normal variate (SNV); multiplicative scatter correction (MSC); logarithmic transformation (LG, based on 10); wavelet transformation (WT); partial least squares − regression (PLS-R); back-propagation neural network (BPNN); the ratio of performance to deviation (RPD); the ratio between the interpretable sum squared deviation and the real sum squared deviation (SSR/SST).

Acknowledgements

The assistance of Liu Zhao, Wencai Wang and Youhua Ma in soil sampling and laboratory physicochemical analysis are gratefully acknowledged. This study has been financed by the International S & T Cooperation Project of the China Ministry of Agriculture (2015-Z44, 2016-X34). The authors also appreciate the financial support received by Haijun Qi from the China Scholarship Council (201608340066).

Appendix A. Supplementary data

Supplementary data associated with this article can be found, in the online version, at http://dx.doi.org/10.1016/j.still.2017.09.006.

References

Adar, S., Shkolnisky, Y., Ben-Dor, E., 2014. Change detection of soils under small-scale laboratory conditions using imaging spectroscopy sensors. Geoderma 216, 19–29. http://dx.doi.org/10.1016/j.geoderma.2013.10.017.

Basheer, I.A., Hajmeer, M., 2000. Artificial neural networks: fundamentals, computing, design, and application. J. Microbiol. Methods 43, 3–31. http://dx.doi.org/10.1016/S0167-7012(00)00201-3.

Ben-Dor, E., Banin, A., 1995. Near-infared analysis as a rapid method to simultaneously evaluate several soil properties. Soil Sci. Soc. Am. J. 59, 364–372. http://dx.doi.org/10.2136/sssaj1995.03615995005900020014x.

Brabanter K., De Karsmakers P., Ojeda F., Alzate C., Brabanter J., De Pelckmans K., Moor B., De Vandewalle J., Suykens J.A.K., 2011, LS-SVMlab Toolbox User's Guide, ESAT-SISTA technical report.

Buddenbaum, H., Steffens, M., 2012. The effects of spectral pretreatments on chemometric analyses of soil profiles using laboratory imaging spectroscopy. Appl. Environ. Soil Sci. 2012. http://dx.doi.org/10.1155/2012/274903.

Cen, H., Lu, R., Zhu, Q., Mendoza, F., 2016. Nondestructive detection of chilling injury in cucumber fruit using hyperspectral imaging with feature selection and supervised classification. Postharvest Biol. Technol. 111, 352–361. http://dx.doi.org/10.1016/j.postharvbio.2015.09.027.

Chang, C.-W., Laird, D.A., Mausbach, M.J., Hurburgh, C.R., 2001. Near-infrared reflectance spectroscopy–principal components regression analyses of soil properties. Soil Sci. Soc. Am. J. 65, 480–490. http://dx.doi.org/10.2136/sssaj2001.652480x.

Chen, G.Q., Jiang, M.M., Yang, Z.F., Chen, B., Ji, X., Zhou, J.B., 2009. Exergetic assessment for ecological economic system: chinese agriculture. Ecol. Modell. 220, 397–410. http://dx.doi.org/10.1016/j.ecolmodel.2008.10.006.

Chen, H., Cao, C., Kong, L., Zhang, C., Li, W., Qiao, Y., 2014. Study on wheat yield stability in huaibei lime concretion black soil area based on long-term fertilization experiment. Sci. Agric. Sin. 47, 2580–2590. http://dx.doi.org/10.3864/j.issn.0578-1752.2014.13.010.

Clark, R.N., King, T.V.V., Klejwa, M., Swayze, G., Vergo, N., 1990. High spectral resolution reflectance spectroscopy of minerals. J. Geophys. Res. 12653–12680.

Confalonieri, M., Fornasier, F., Ursino, A., Boccardi, F., Pintus, B., Odoardi, M., 2001. The potential of near infrared reflectance spectroscopy as a tool for the chemical characterisation of agricultural soils. J. Near Infrared Spectrosc. 9, 123–131. http://dx.doi.org/10.1255/jnirs.299.

Cope, M., van der Zee, P., Essenpreis, M., Arridge, S.R., Delpy, D.T., 1991. Data analysis methods for near-infrared spectroscopy of tissue: problems in determining the relative cytochrome aa3 concentration. Optics, Electro-Optics, and Laser Applications in Science and Engineering. International Society for Optics and Photonics, pp. 251–262. http://dx.doi.org/10.1017/CBO9781107415324.004.

Dong, G., Guo, J., Wang, C., Chen, Z.L., Zheng, L., Zhu, D.Z., 2015. The classification of wheat varieties based on near infrared hyperspectral imaging and information fusion. Spectrosc. Spectr. Anal. 35, 3369–3374. http://dx.doi.org/10.3964/j.issn.1000-0593(2015)12-3369-06.

Galvão, L.S., Vitorello, Í., Formaggio, A.R., 1997. Relationships of spectral reflectance and color among surface and subsurface horizons of tropical soil profiles. Remote Sens. Environ. 61, 24–33. http://dx.doi.org/10.1016/S0034-4257(96)00219-2.

Gholizade, A., Soom, M.A.M., Saberioon, M.M., Borůvk, P.L., 2013. Visible and near infrared reflectance spectroscopy to determine chemical properties of paddy soils. J. Food Agric. Environ. 11, 859–866.

Gholizadeh, A., Boruvka, L., Saberioon, M.M., Kozák, J., Vašát, R., Nemecek, K., 2015. Comparing different data preprocessing methods for monitoring soil heavy metals based on soil spectral features. Soil Water Res. 10, 218–227. http://dx.doi.org/10.17221/113/2015-SWR.

Gras, J.P., Barthès, B.G., Mahaut, B., Trupin, S., 2014. Best practices for obtaining and processing field visible and near infrared (VNIR) spectra of topsoils. Geoderma 214–215, 126–134. http://dx.doi.org/10.1016/j.geoderma.2013.09.021.

He, T., Wang, J., Lin, Z., Cheng, Y., 2009. Spectral features of soil organic matter. Geo-Spatial Inf. Sci. 12, 33–40. http://dx.doi.org/10.1007/s11806-009-0160-x.

Helland, I.S., Næs, T., Isaksson, T., 1995. Related versions of the multiplicative scatter correction method for preprocessing spectroscopic data. Chemom. Intell. Lab. Syst. 29, 233–241. http://dx.doi.org/10.1016/0169-7439(95)80098-T.

Hsu, C.-W., Chang, C.-C., Lin, C.-J., 2008. A practical guide to support vector classification [WWW document]. BJU Int. http://dx.doi.org/10.1177/02632760022050997.

Hu, G., Sudduth, K.A., He, D., Myers, D.B., Nathan, M.V., 2016. Soil phosphorus and potassium estimation by reflectance spectroscopy. Trans. ASABE 59, 97–105. http://dx.doi.org/10.13031/trans.59.11048.

Hunt, G.R., Salisbury, J.W., 1970. Visible and near-infrared spectra of minerals and rocks: I. silicate minerals. Mod. Geol. 1, 282–300.

Janik, L.J., Cozzolino, D., Dambergs, R., Cynkar, W., Gishen, M., 2007. The prediction of total anthocyanin concentration in red-grape homogenates using visible-near-infrared spectroscopy and artificial neural networks. Anal. Chim. Acta 594, 107–118. http://dx.doi.org/10.1016/j.aca.2007.05.019.

Ji, W., Shi, Z., Huang, J., Li, S., 2014. In situ measurement of some soil properties in paddy soil using visible and near-infrared spectroscopy. PLoS One 9, e105708. http://dx.doi.org/10.1371/journal.pone.0105708.

Jung, A., Vohland, M., Thiele-Bruhn, S., 2015. Use of a portable camera for proximal soil sensing with hyperspectral image data. Remote Sens. 7, 11434–11448. http://dx.doi.org/10.3390/rs70911434.

Kennard, R.W., Stone, L.A., 1969. Computer aided design of experiments. Technometrics 11, 137–148. http://dx.doi.org/10.1080/00401706.1969.10490666.

Kvalseth, T.O., 1985. Cautionary note about R 2. Am. Stat. 39, 279. http://dx.doi.org/10.2307/2683704.

Li, S., Wang, S., Shi, Z., 2015. Prediction of vertical distribution of soil nitrogen content in soil profile using spectral imaging technique. Acta Pedol. Sin. 52, 1014–1023. http://dx.doi.org/10.11766/trxb201409030442.

Lu, R.K., 2000. Methods of Soil and Agrochemistry Analysis. China Agricultural Science and Technology Press, Beijing.

Ma, C., Shao, X., 2004. Continuous wavelet transform applied to removing the fluctuating background in near-infrared spectra. J. Chem. Inf. Comput. Sci. 44, 907–911. http://dx.doi.org/10.1021/ci034211+.

Ma, Y., Li, X., Li, D., Han, Z., Zhang, G., Zhang, W., Hu, C., Shao, Y., 2014. Spatial variation of soil organic carbon content in farmland and its influencing factors in Mengcheng County, Northern Anhui Plain. Acta Pedol. Sin. 51, 1153–1159.

McGill, R., Tukey, J.W., Larsen, W.A., 1978. Variations of box plots. Am. Stat. 32, 12. http://dx.doi.org/10.2307/2683468.

Morellos, A., Pantazi, X.-E., Moshou, D., Alexandridis, T., Whetton, R., Tziotzios, G., Wiebensohn, J., Bill, R., Mouazen, A.M., 2016. Machine learning based prediction of soil total nitrogen, organic carbon and moisture content by using VIS-NIR spectroscopy. Biosyst. Eng. 152, 1–13. http://dx.doi.org/10.1016/j.biosystemseng.2016.04.018.

Mouazen, A.M., Kuang, B., De Baerdemaeker, J., Ramon, H., 2010. Comparison among principal component, partial least squares and back propagation neural network analyses for accuracy of measurement of selected soil properties with visible and near infrared spectroscopy. Geoderma 158, 23–31. http://dx.doi.org/10.1016/j.geoderma.2010.03.001.

O'Rourke, S.M., Holden, N.M., 2012. Determination of soil organic matter and carbon fractions in forest top soils using spectral data acquired from visible–near infrared hyperspectral images. Soil Sci. Soc. Am. J. 76, 586. http://dx.doi.org/10.2136/sssaj2011.0053.

Osborne, B.G., Fearn, T., Hindle, P.H., 1993. Practical NIR Spectroscopy with Applications in Food and Beverage Analysis. Longman Scientific and Technical Addison-Wesley Longman Ltd.

Osborne, J.W., 2000. Prediction in multiple regression. Pract. Assessment Res. Eval. 7, 1–6.

Pang, G., Wang, T., Liao, J., Li, S., 2014. Quantitative model based on field-derived spectral characteristics to estimate soil salinity in minqin county. China. Soil Sci. Soc. Am. J. 78, 546–555. http://dx.doi.org/10.2136/sssaj2013.06.0241.

Paz-Kagan, T., Shachak, M., Zaady, E., Karnieli, A., 2014. A spectral soil quality index (SSQI) for characterizing soil function in areas of changed land use. Geoderma 230–231, 171–184. http://dx.doi.org/10.1016/j.geoderma.2014.04.003.

Paz-Kagan, T., Zaady, E., Salbach, C., Schmidt, A., Lausch, A., Zacharias, S., Notesco, G., Ben-Dor, E., Karnieli, A., 2015. Mapping the spectral soil quality index (SSQI) using airborne imaging spectroscopy. Remote Sens. 7, 15748–15781. http://dx.doi.org/10.3390/rs71115748.

Peng, J., Shen, H., He, S.W., Wu, J.S., 2013. Soil moisture retrieving using hyperspectral data with the application of wavelet analysis. Environ. Earth Sci. 69, 279–288. http://dx.doi.org/10.1007/s12665-012-1955-x.

Peng, X., 2010. TSVR: an efficient twin support vector machine for regression. Neural Netw. 23, 365–372. http://dx.doi.org/10.1016/j.neunet.2009.07.002.

Rinnan, Å., Berg, F., van den Engelsen, S.B., 2009. Review of the most common pre-processing techniques for near-infrared spectra, TrAC. Trends Anal. Chem. 28, 1201–1222. http://dx.doi.org/10.1016/j.trac.2009.07.007.

Roberts, C.A., Workman Jr., J., Reeves III., J.B., Duckworth, J., 2004. Mathematical data preprocessing. Near-Infrared Spectroscopy in Agriculture. American Society of Agronomy, Crop Science Society of America, Soil Science Society of America, pp. 115–132. http://dx.doi.org/10.2134/agronmonogr44.c6.

Rourke, S.M.O., Holden, N.H., 2012. Determination of soil organic matter and carbon fractions in forest top soils using spectral data acquired from visible–near infrared hyperspectral images. Soil Sci. Soc. Am. J. 76, 586. http://dx.doi.org/10.2136/sssaj2011.0053.

Sadowski, A., Scibisz, K., Tomala, K., 1987. Negative effects of excessive nitrogen and potassium fertilization in a replanted apple orchard. Work. Replant.

Saeys, W., Darius, P., Ramon, H., 2004. Potential for on-site analysis of hog manure using a visual and near infrared diode array reflectance spectrometer. J. Near Infrared Spectrosc. 12, 299–309. http://dx.doi.org/10.1255/jnirs.438.

Sarathjith, M., Das, B., Wani, S., Sahrawat, K.L., Gupta, A., 2016. Comparison of data mining approaches for estimating soil nutrient contents using diffuse reflectance spectroscopy. Curr. Sci. 110, 1031–1037. http://dx.doi.org/10.18520/cs/v110/i6/1031-1037.

Savci, S., 2012. An agricultural pollutant: chemical fertilizer. Int. J. Environ. Sci. Dev. 3, 11–14. http://dx.doi.org/10.7763/IJESD.2012. V3.191.

Savitzky, A., Golay, M.J.E., 1964. Smoothing and differentiation of data by simplified least squares procedures. Anal. Chem. 36, 1627–1639. http://dx.doi.org/10.1021/ac60214a047.

Shaddad, S.M., Madrau, S., Castrignanò, A., Mouazen, A.M., 2016. Data fusion techniques for delineation of site-specific management zones in a field in UK. Precis. Agric. 17, 200–217. http://dx.doi.org/10.1007/s11119-015-9417-6.

Shao, Y., He, Y., 2011. Nitrogen, phosphorus, and potassium prediction in soils, using infrared spectroscopy. Soil Res. 49, 166–172. http://dx.doi.org/10.1071/SR10098.

Shi, T., Cui, L., Wang, J., Fei, T., Chen, Y., Wu, G., 2013. Comparison of multivariate methods for estimating soil total nitrogen with visible/near-infrared spectroscopy. Plant Soil 366, 363–375. http://dx.doi.org/10.1007/s11104-012-1436-8.

Shmueli, G., 2010. To explain or to predict? Stat. Sci. 25, 289–310. http://dx.doi.org/10.1214/10-STS330.

Soriano-Disla, J.M., Janik, L.J., Viscarra Rossel, R.A., MacDonald, L.M., McLaughlin, M.J., 2014. The performance of visible, near-, and mid-infrared reflectance spectroscopy for prediction of soil physical, chemical, and biological properties. Appl. Spectrosc. Rev. 49, 139–186. http://dx.doi.org/10.1080/05704928.2013.811081.

Spiess, A.-N., Neumeyer, N., 2010. An evaluation of R2 as an inadequate measure for nonlinear models in pharmacological and biochemical research: a Monte Carlo approach. BMC Pharmacol. 10, 6. http://dx.doi.org/10.1186/1471-2210-10-6.

Stenberg, B., Viscarra Rossel, R.A., Mouazen, A.M., Wetterlind, J., 2010. Visible and near infrared spectroscopy in soil science. Adv. Agron. http://dx.doi.org/10.1016/S0065-2113(10)07005-7.

Stoner, E.R., Baumgardner, M.F., 1980. Physicochemical, Site, and Bidirectional Reflectance Factor Characteristics of Uniformly Moist Soils, AgRISTARS. West Lafayette, IN, United States.

Suykens, J.A.K., Van Gestel, T., De Brabanter, J., De Moor, B., Vandewalle, J., 2002. Least Squares Support Vector Machines. World Scientific.

Tian, Y., Zhang, J., Yao, X., Cao, W., Zhu, Y., 2013. Laboratory assessment of three quantitative methods for estimating the organic matter content of soils in China based on visible/near-infrared reflectance spectra. Geoderma 202–203, 161–170. http://dx.doi.org/10.1016/j.geoderma.2013.03.018.

Tong, L., Zhou, J., Xu, C., Qian, Y., Gao, Y., 2013. Soil biochar quantification via hyperspectral unmixing. 2013 Int. Conf. Digit. Image Comput. Tech. Appl. DICTA 2013. 10.1109/DICTA.2013.6691529.

Viscarra Rossel, R.A., Walvoort, D.J.J., McBratney, A.B., Janik, L.J., Skjemstad, J.O., 2006. Visible, near infrared, mid infrared or combined diffuse reflectance spectroscopy for simultaneous assessment of various soil properties. Geoderma 131, 59–75. http://dx.doi.org/10.1016/j.geoderma.2005.03.007.

Weisberg, S., 2005. Applied Linear Regression, 3rd ed. John Wiley & Sons, Inc.http://dx.doi.org/10.1002/0471704091.

Wen, W., Hao, Z., Yang, X., 2008. A heuristic weight-setting strategy and iteratively updating algorithm for weighted least-squares support vector regression. Neurocomputing 3096–3103. http://dx.doi.org/10.1016/j.neucom.2008.04.022.

Westad, F., Marten, H., Martens, H., 2000. Variable selection in near infrared spectroscopy based on significance testing in partial least squares regression. J. Near Infrared Spectrosc. 8, 117–124. http://dx.doi.org/10.1255/jnirs.271.

Widyanto, M.R., Nobuhara, H., Kawamoto, K., Hirota, K., Kusumoputro, B., 2005. Improving recognition and generalization capability of back-propagation NN using a self-organized network inspired by immune algorithm (SONIA). Appl. Soft Comput. J. 6, 72–84. http://dx.doi.org/10.1016/j.asoc.2004.10.008.

Wold, S., Martens, H., Wold, H., 1983. The multivariate calibration problem in chemistry solved by the PLS method. In: Kågström, B., Ruhe, A. (Eds.), Matrix Pencils. Lecture Notes in Mathematics. Springer, Berlin, Heidelberg, pp. 286–293. http://dx.doi.org/10.1007/BFb0062108.

Wold, S., Ruhe, A., Wold, H., Dunn Jr., W.J., 1984. The collinearity problem in linear regression. The partial least squares (PLS) approach to generalized inverses. SIAM J. Sci. Stat. Comput. 5, 735–743. http://dx.doi.org/10.1137/0905052.

Wu, Q., Yang, Y., Xu, Z., Jin, Y., Guo, Y., Lao, C., 2014. Applying local neural network and visible/near-infrared spectroscopy to estimating available nitrogen, phosphorus and potassium in soil. Spectrosc. Spectr. Anal. 34, 2102–2105. http://dx.doi.org/10.3964/j.issn.1000-0593(2014)08-2102-04.

Xavier-De-Souza, S., Suykens, J.A.K., Vandewalle, J., Bolle, D., 2010. Coupled simulated annealing. IEEE Trans. Syst. Man, Cybern. Part B Cybern. 40, 320–335. http://dx.doi.org/10.1109/TSMCB.2009.2020435.

Yu, X., Liu, Q., Wang, Y., Liu, X., Liu, X., 2016. Evaluation of MLSR and PLSR for estimating soil element contents using visible/near-infrared spectroscopy in apple orchards on the Jiaodong peninsula. Catena 137, 340–349. http://dx.doi.org/10.1016/j.catena.2015.09.024.